FULL PAPER

HELVETICA
chimica acta

Anionic Thia-*Fries* Rearrangement at Ferrocene: A Computational and Experimental Study

Geanne M. R. Boston,[a] Irmgard Frank,*[b] and Holger Butenschön*[a]

[a] Institut für Organische Chemie, Leibniz Universität Hannover, Schneiderberg 1B, D-30167 Hannover, Germany, e-mail: holger.butenschoen@mbox.oci.uni-hannover.de
[b] Institut für Physikalische Chemie und Elektrochemie, Leibniz Universität Hannover, Callinstraße 3a, D-30167 Hannover, Germany, e-mail: irmgard.frank@theochem.uni-hannover.de

Dedicated to Professor Dr. *E. Peter Kündig* on the Occasion of his 75th Birthday

Ferrocenyl triflate (**1**) and 1,1′-ferrocenediyl ditriflate (**5**) undergo single and double anionic thia-*Fries* rearrangements at low temperatures in high yields with the latter forming exclusively the respective *meso* product. The detailed mechanisms of the anionic thia-*Fries* rearrangement of **1**, as well as that of the double anionic thia-*Fries* rearrangement of **5**, are examined with the aid of DFT calculations. Functionals, basis set and pseudopotentials applied were selected in accordance with a benchmark using the crystal structure analysis of the prime product **3** of the reaction of **1** before hydrolysis for comparison, which has so far not been reported. The unprecedented *meso* diastereoselectivity of the double anionic thia-*Fries* rearrangement of **5** is shown to be a result of a distinctive degree of chelation arising from two diastereomeric transition states.

Keywords: anionic thia-Fries rearrangement, crystal structure analysis, density functional calculations, ferrocenyl triflates, reaction mechanisms.

Introduction

The anionic thia-*Fries* rearrangement of aryl triflates (1,3-$O_{Ar} \rightarrow C_{Ar}$ migration) was first published by *Lloyd-Jones* and coworkers in 2003,[1] and since then it has been shown to also take place in $Cr(CO)_3$ complexes with η^6-aryl triflates[2] and ferrocenyl triflates.[3] The rearrangement in $Cr(CO)_3$ complexes is in agreement with the first findings of *Lloyd-Jones* and coworkers, showing partition between rearrangement and benzyne generation due to an electron withdrawing or donating group *ortho* to the triflate group, respectively. However, the rearrangement of the electron rich ferrocenyl triflate (**1**) leading to 1-hydroxy-2-(trifluoromethyl)ferrocene (**4**, *Scheme 1*) presumably through **2** and **3**, which was published in 2010 by
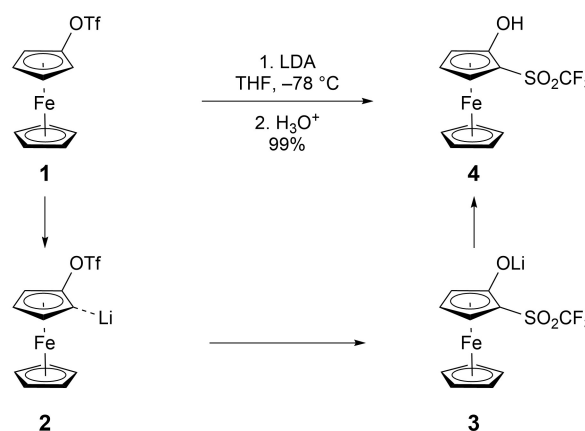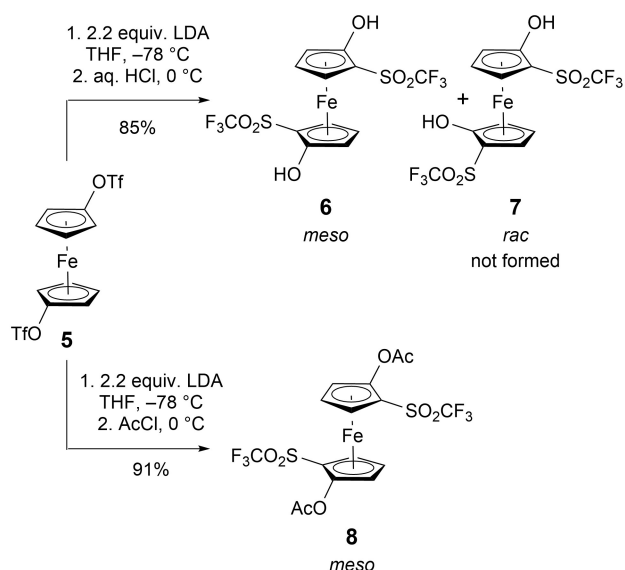
Scheme 1. Anionic thia-*Fries* rearrangement of ferrocenyl triflate (**1**).[3]

Butenschön and coworkers,[3] takes place instantaneously at low temperatures contradicting this assump-

tion. The first mechanistic study involved isotopically labelled aryl triflates and gas phase DFT [B3LYP/6-31G (d)] calculations. This study showed that the rearrangement proceeds by an intramolecular anionic $O_{Ar} \rightarrow C_{Ar}$ transfer of the SO_2CF_3 group through a single transition state, and that the *ortho* C–H cleavage is irreversible.[4]

A double thia-*Fries* rearrangement in 1,1′-ferrocenediyl ditriflate (**5**) with full diastereoselectivity was observed by Butenschön and coworkers (*Scheme 2*).[3] The origin of the selective formation of the *meso* product **6** trapped as diacetate **8** with no *rac* product **7** being obtained is still unknown. Herein, we report experimental and computational investigations of the

anionic thia-*Fries* rearrangement in ferrocenyl triflate (**1**) and 1,1′-ferrocenediyl ditriflate (**5**) and unravel the origin of the observed diastereoselectivity.

Results and Discussion

A number of bases for the rearrangement of **1** were screened in order to obtain a better insight into the importance of the counter cation and the solvent (*Table 1*). Furthermore, it was hoped that the formation of 1,2-dehydroferrocene (ferrocyne) would be observed, which was, unfortunately not the case. The use of lithium diisopropylamide (LDA) in the presence of 12-crown-4 did not change the result nor the yield of the reaction. Using the sodium analogue of LDA, NaDA,[5] also led to the rearrangement product, albeit in a lower yield. However, significantly lower yields were observed when either sodium or potassium bis (trimethylsilyl)amide were used suggesting that the counter cation charge density might indeed play an important role.

The use of diisopropylamine (DIPA) instead of THF as the solvent led to a lower yield, but only the rearrangement product **4** was formed. Based on the conclusions of *Lloyd-Jones* and coworkers,[1] the use of DIPA was expected to cause the elimination of the triflate group with the formation of 1,2-dehydroferrocene (ferrocyne). The use of hydride bases, NaH and KH, led to a nucleophilic attack with the formation of hydroxyferrocene.

Although many more bases could have been tested to better understand the complex system formed between ferrocenyl triflates and amide bases, detailed computational studies seemed to be a more promising

Scheme 2. Diastereoselective double anionic thia-*Fries* rearrangement of 1,1′-ferrocenediyl ditriflate (**5**).[3]

Table 1. Screening of different bases for the anionic thia-*Fries* rearrangement of ferrocenyl triflate (**1**).

Base (1 equiv.)	Conditions	Yield of **2** [%]	Recovered **1** [%]
LDA[a]	THF, −78 °C→23 °C, 30 min	99	–
LDA/12-crown-4	THF, −78 °C→23 °C, 30 min	99	–
LDA	DIPA, −78 °C→23 °C, 30 min	75	13
NAH	THF, 23 °C, 16 h	–[b]	–
KH	THF, 23 °C, 16 h	–[b]	–
NaDA[5]	THF, −78 °C, 40 min	81[c]	–
NaN[Si(CH$_3$)$_3$)]$_2$	0 °C→23 °C, 16 h	62	–
KN[Si(CH$_3$)$_3$]$_2$	0 °C→23 °C, 16 h	13	67
Phosphazene P2-*t*Bu	THF, −78 °C→0 °C, 30 min	–[d]	61
Mg(DA)$_2$	THF, −78 °C→0 °C, 30 min	–[e]	29

[a] Benchmark[3]. [b] Hydroxyferrocene formed. [c] Product quenched with AcCl. [d] 24 % Hydroxyferrocene quenched with AcCl. [e] 4 % Hydroxyferrocene quenched with AcCl.

approach. Meanwhile, the primary thia-*Fries* rearrangement product **3** (*Figure 1*[1]) before hydrolysis was isolated in 96% yield as a highly air and moisture sensitive solid (*Scheme 1*). Crystals suitable for an X-ray crystal structure analysis were obtained through solvent diffusion. In addition to being an interesting aggregate in itself, its crystal structure provided a good way to benchmark the theoretical analysis.

Lithium has a high charge density compared to larger cations and shows a tendency to form contact ion pairs,[6] which explains the self-assembly observed in the X-ray crystallographic analysis. In this structure, the lithium atoms are strongly bound to the alkoxide and one of the sulfonyl oxygen atoms forming a six-
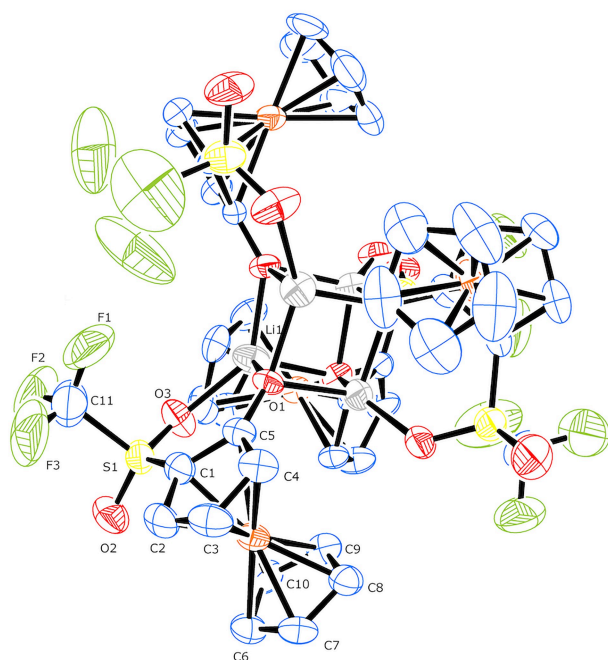

Figure 1. Structure of **3** in the crystal.[1] Ellipsoids at 50% probability level. Hydrogen atoms have been omitted for clarity. Within the formed cube, the Li–O bond distances vary from 192.8(9) pm to 196.2(9) pm; the O–Li–O angles range from 91.3(3)° to 96.6(4)° and Li–O–Li from 83.3(4)° to 97.7(4)°. Selected bond lengths [pm]: Fe1–C1 201.0(5), Fe1–C2 201.4(5), Fe1–C3 204.7(5), Fe1–C4 208.8(5), Fe1–C5 212.6(5), Fe1–C6 206.4(5), Fe1–C7 204.5(6), Fe1–C8 205.3(5), Fe1–C9 205.2(5), Fe1–C10 204.3(5), C1–S1 171.4(5), S1–O2 142.2(4), S1–O3 143.3(4), S1–C11 184.1(8), C11–F1 128.9(8), C11–F2 131.3(8), C11–F3 133.2(9), C5–O1 130.0(5), O1–Li1 195.9(8), Li1–O3 198.2(9).

---

[1] CCDC-2046411 contains the supplementary crystallographic data for this article. These data can be obtained free of charge from *The Cambridge Crystallographic Data Centre* through https://www.ccdc.cam.ac.uk/structures/.

membered chelate ring. The O–Li moiety originating from the migration of the sulfonyl group interacts strongly with two other O–Li moieties forming a heterocubane structure of four lithium and four oxygen atoms (Li_4O_4). While this motif is quite common for alkali metal alkoxides with bulky substituents,[7] there are only few structures known, which involve ferrocene moieties.[8,9]

Molecular dynamic simulations were carried out using the CPMD method[10] and software package.[11] The functionals, basis set and pseudopotential were chosen accordingly to benchmarks performed for both CPMD and *Gaussian* software using the X-Ray crystal structure of **3** for comparison. The full benchmarks descriptions, graphs comparing the performance of the functional and the full direct comparison table of the bond lengths are available in the *Supporting Information*. The chosen functional for the CPMD calculations was PBE, whilst the hybrid PBE0 was used for the *Gaussian* studies.

LDA was included in the *Gaussian* model of the mono- and double rearrangements. An implicit solvent and a molecule of THF were additionally included in the mono rearrangement model. This was not possible for the double rearrangement, as some steps in the reaction pathway were not found when the continuum solvent and a molecule of THF were present. This differs from the work of *Lloyd-Jones*,[4] which used no base, an already *ortho*-deprotonated phenyl triflate and an implicit solvent. Although the base increases complexity, it better models the intricate pathways and intermediate organolithium structures of the reaction.

The strategy devised in this study to obtain the transition state structures in *Gaussian*, was to perform a relaxed scan, followed by an optimization of the structures at the highest point of the curve. After finding the desired structures, it was verified that only one imaginary negative vibrational frequency was present (saddle point), and the corresponding eigenvector visualized to check for consistency with the expected chemical reaction. An intrinsic reaction coordinate (IRC) calculation was performed afterwards to verify if the obtained transition state led to the desired product and back to the reactant connecting both of them.

Based on the calculations, we propose the mechanism of the anionic thia-*Fries* rearrangement of ferrocenyl triflate (**1**) depicted in *Figure 2*. Calculations using two explicit THF molecules were performed for the starting structure **A** and transition state **B** but did not lead to significant differences. Calculations for
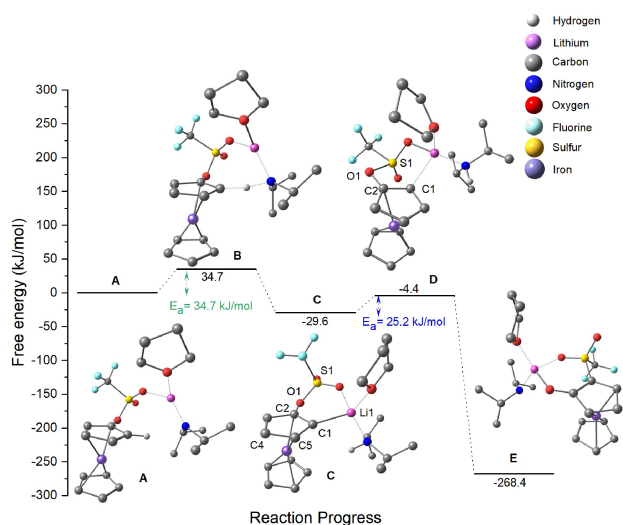
Figure 2. Relative free-energy scheme for the deprotonation and rearrangement of ferrocenyl triflate (**1**) at the PBE0/[LANL2DZ/LANL2/6-311 + G(*d,p*)] level of theory. Most of the hydrogen atoms have been omitted for clarity.

intermediate **C** using two THF molecules did not converge. The modelling of this reaction shows a strong coordination between reactant, lithium base and solvent, forming a pre-complex **A** as shown in the energy diagram (*Figure 2*). It is interesting to note, that the lithium atom is coordinated to THF and the sulfonyl oxygen atoms. The transition structure **B** reveals a low barrier with a small activation energy of 34.7 kJ/mol and has a geometry very similar to that of **A**, except that the amide now interacts with the *ortho* proton. The angle N—H—C involved in the proton transfer step is 168°.

The intermediate structure **C** found shows an intramolecular chelation of the lithium ion with one of the oxygen atoms of the triflate group, and coordinates to THF and to the previously formed diisopropylamine. The energy released is only 29.6 kJ/mol, being mildly exothermic. *Lloyd-Jones* and coworkers decouple deprotonation from metalation and concluded that metalation *ortho* to a triflate group results in elimination and deprotonation alone to thia-*Fries* rearrangement.[4] Following this reasoning, *Butenschön* and *Werner* tested how far *ortho* lithiation instead of *ortho* deprotonation in ferrocene could shift the results. 2-Tributylstannylferrocenyl triflate was treated with butyllithium in the presence of 2,5-diphenylisobenzofuran, which should have been followed by metal exchange and expected to undergo elimination forming ferrocyne. Instead, the anionic thia-*Fries* rearrangement immediately took place.[12] There was

also no sign of elimination and formation of ferrocyne, when **1** was treated with LDA;[3] however, **C** does suggest *ortho* metalation. The bond distance C1—Li1 is 210 pm, smaller than the distance C—Li of 231 pm in methyllithium,[13] and smaller than the sum of the atomic radii of C (70 pm) and Li (145 pm), 215 pm.[14] The dihedral angle Li1—C1—C5—C4 is 161°. The HOMO of **C** was also analyzed, and a bonding interaction along the C1—Li1 distance was observed as shown in *Figure 3*.

Maximally localized *Wannier* Functions (MLWF) were also calculated using CPMD software package.[11] These localized orbitals allow to analyze the electronic structure. A localized orbital was found between C1 and Li1 suggesting a putative heavily polarized covalent bond (*Figure 4*).

The rearrangement transition state proceeds through $(1,3-O_{Ar} \rightarrow C_{Ar})$ sulfonyl migration with an average activation energy of 58.3 kJ/mol. The reaction is highly exothermic (238.7 kJ/mol). The transition structure **D** shows a dihedral angle C1—C2—O1—S1 of 3°, which is close to planarity. The distance C2—O1 decreases to 137 pm compared to 144 pm in **C**, whilst O1—S1 increases to 172 pm compared to the corresponding distance of 157 pm in **C**. The distance S1—C1 changes a lot, partially due to the change in conformation, from 327 pm in **C** to 230 pm in the transition state **D**. The product **E**, although still
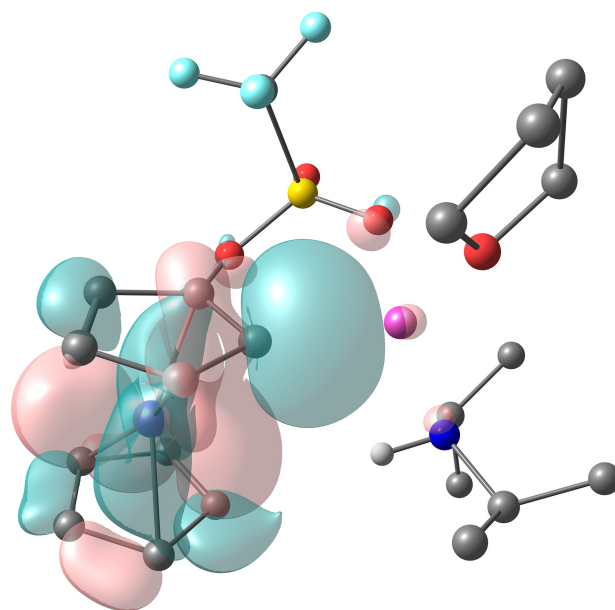

Figure 3. HOMO of the intermediate **C**. For atom color code, see *Figure 2*. Most of the hydrogen atoms have been omitted for clarity. The color of the isosurface refers to the sign/phase: Positive for red and negative for green.
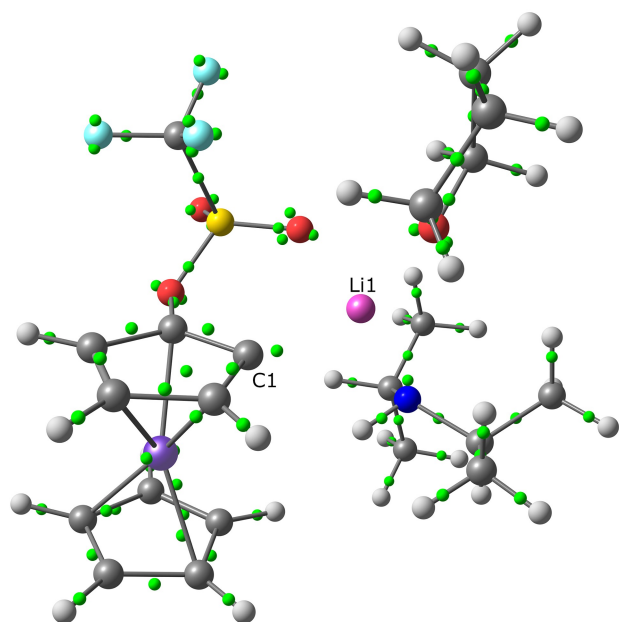
HELVETICA
chimica acta

Figure 4. MLWF of intermediate **C**. For atom color code see *Figure 2*. Green spheres represent localized orbitals centers.

Figure 5. Relative free-energy scheme for the first deprotonation and rearrangement of 1,1'-ferrocenediyl ditriflate (**5**) at PBE0/[LANL2DZ/LANL2/ 6-311+G(d,p)] level of theory. Most of the hydrogen atoms have been omitted for clarity.

coordinated to THF and diisopropylamine, shows a structure very similar to the subunits of the tetramer revealed in the X-ray crystal analysis (*Figure 1*).

The mechanistic studies of the double anionic thia-*Fries* rearrangement of 1,1'-ferrocenediyl ditriflate (**5**) using LDA as the base are subdivided into two potential energy diagrams including calculated structures of reactants, intermediates, transition states and product in a stepwise fashion. The first one, shown in *Figure 5*, represents the computational results regarding the first deprotonation, followed by the first rearrangement at one of the cyclopentadienyl rings. The second one, shown in *Figure 6*, reveals the second deprotonation followed by the second rearrangement. A concerted mechanism was considered, but no respective transition state was found.

The model used for the double anionic thia-*Fries* rearrangement of **5** to **12** through **9**–**11** (*Scheme 3*) did not use implicit solvent and a molecule of THF as described for the mono rearrangement. The transition states of the rearrangement steps were not found using implicit solvent and were even less successful with a molecule of THF. The reason why it was difficult to find it, is probably due to a very low imaginary vibrational frequency (-131 cm^{-1} for **I** and -171 cm^{-1} for **O**), which means that it lies on a very flat potential energy surface (second derivative corresponds to curvature) and that the addition of solvent adds more degrees of freedom making it more difficult to find the desired structure.
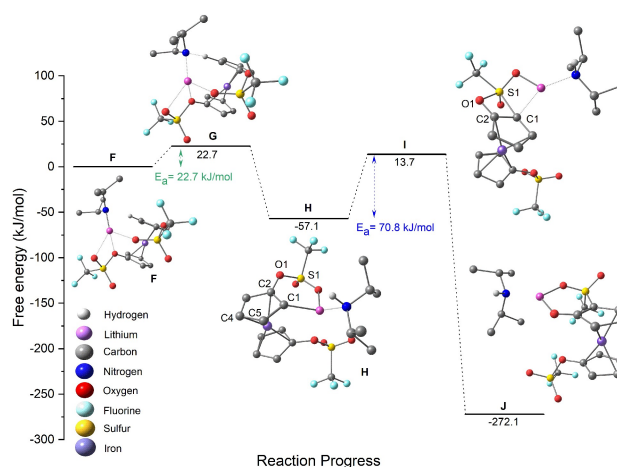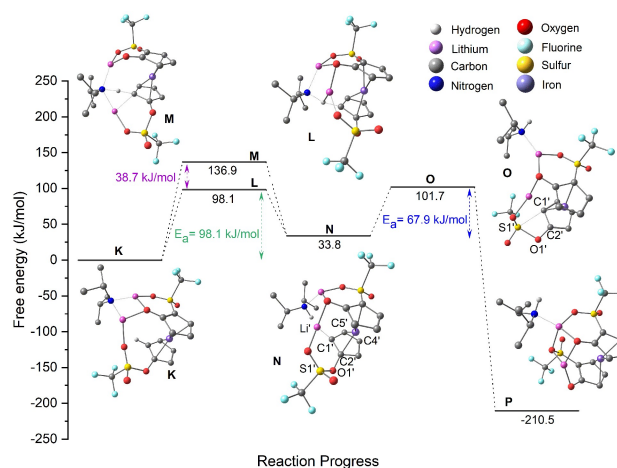

Figure 6. Relative free-energy scheme for the second deprotonation and rearrangement of 1,1'-ferrocenediyl ditriflate (**5**) at PBE0/[LANL2DZ/ LANL2/6-311+G(d,p)] level of theory. Most of the hydrogen atoms have been omitted for clarity.

The calculations for the first transition state and rearrangement of **5** depicted in *Figure 5*, starts with 1,1'-ferrocenediyl ditriflate (**5**) also as a pre-complex **F**, strongly coordinated to LDA. The transition state structure **G** has a geometry similar to that of **F** and a very small activation barrier of 22.7 kJ/mol. The proton transfer angle N–H–C is 172°. In the intermediate structure **H** it is possible to see that an *ortho* metalation does not seem to have taken place as in the case of the mono triflate **1**. Rather, the lithium atom is chelated between the oxygen atoms of both triflate groups and the previously formed diisopropylamine.
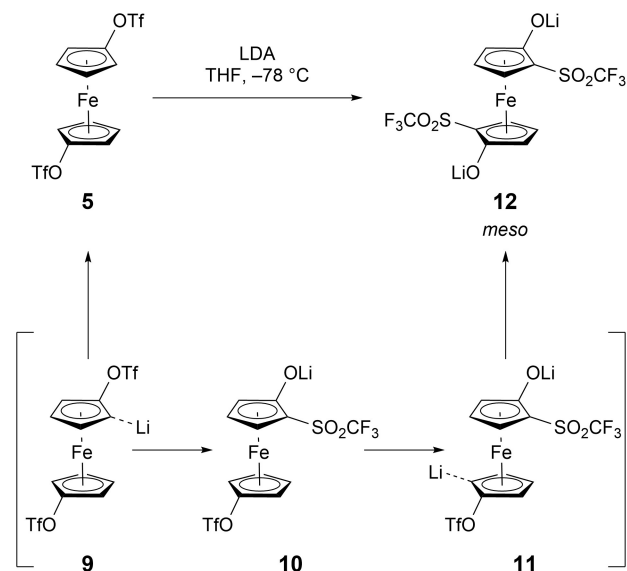
Scheme 3. Double anionic thia-*Fries* rearrangement of 1,1′-ferrocenediyl ditriflate (**5**).

The relative free energy of 57.1 kJ/mol released is not very high.

The rearrangement transition state following after depicts a very similar structure to the mono case (*cf. Figure 2*), proceeding through (1,3-O_{Ar}→C_{Ar}) sulfonyl migration with a medium activation energy of 70.8 kJ/mol. The reaction is highly exothermic. The transition state **I** shows a dihedral angle C1–C2–O1–S1 of 0.4° corresponding to planarity. The distance C2–O1 decreases to 136 pm compared to 143 pm in **H**, whilst the distance O1–S1 increased to 177 pm compared to 158 pm in **H**. The distance S1–C1 changed a lot from 332 pm in **H** to 218 pm in the transition state **I**.

The modelling of the reaction step for the second cyclopentadienyl ligand started with the pre-complex structure **K**, optimized from structure **J** without previously formed DIPA but including an additional LDA. Gratifyingly, the conformation of the formed structure **K** already gave us a clue of the reason for the diastereoselective formation of the *meso* product **12**. Two transition states were found for the deprotonation step, both leading to the observed *meso* product. The main difference between transition state structures **M** and **L** is the degree of intramolecular chelation of lithium atoms. In the first, the lithium atom from LDA is bound only to the oxygen atom of the sulfonyl group of the bottom cyclopentadienyl ring, whilst the second is also chelated by the olate oxygen atom. The difference in energy between them of 38.7 kJ/mol is quite significant and the latter, **L**, most stable, will be

considered for this study. The activation energy of 98.1 kJ/mol for the second deprotonation is much higher than that observed for the first deprotonation, $E_a = 22.7$ kJ/mol (*Figure 5*). The intermediate **N** has a higher energy than **K**, and this reaction step is mildly endothermic. In the intermediate **N**, the distance C1′-Li′ is 208 pm, surprisingly the same distance obtained for structure **H**. The dihedral angle Li′–C1′–C5′–C4′ is 117 °, also far from planarity. It is again inconclusive if metalation occurs, or if the lithium atom is just coordinated between the alcoholate, one of the oxygen atoms of the remaining triflate group and the newly formed diisopropylamine.

The rearrangement transition structure is very similar to its precedent intermediate **N**. It proceeds again through (1,3-O_{Ar}→C_{Ar}) sulfonyl migration with an average activation energy of 67.9 kJ/mol. The reaction is highly exothermic. The transition structure **O** shows a dihedral angle C1–C2–O1–S1 of 2°, which is close to planarity. The distance C2–O1 decreases to 134 pm compared to 143 pm in **N**, whilst the distance O1–S1 increased to 177 pm compared to 158 pm in **N**. The distance S1–C1 significantly changed from 338 pm in **N** to 244 pm in the transition state **O**.

The structure of the transition state leading to the *racemo* product **Q** was calculated and compared. *Figure 7* shows that the planar chirality of the intermediate molecule leads to two different deprotonation transition state geometries. Each diastereomer has a distinctive degree of chelation leading to an impressive difference in energy between them: 59 kJ/mol. This explains the exclusive formation of the *meso* product **12**.
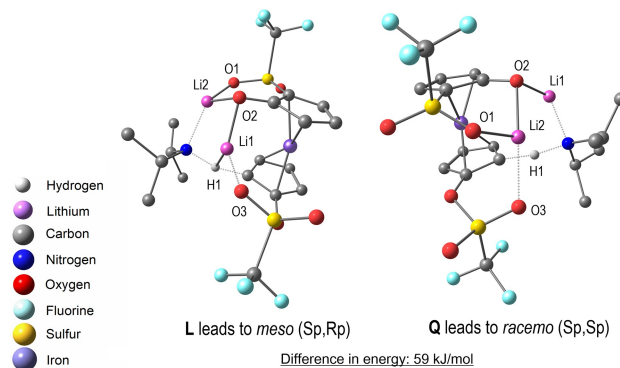

Figure 7. *meso vs. racemo*: Transition state of the second deprotonation in the double anionic thia-*Fries* rearrangement of 1,1′-ferrocenediyl ditriflate (**5**). Most of the hydrogen atoms have been omitted for clarity.

Conclusions

In conclusion, the detailed mechanisms of the anionic thia-*Fries* rearrangement of ferrocenyl triflate (**1**) as well as that of the double anionic thia-*Fries* rearrangement of 1,1′-ferrocendiyl ditriflate (**5**) have been investigated by DFT calculations. The functionals, basis set and pseudopotentials applied were selected on the basis of the crystal structure analysis of the prime product **3** of the reaction of **1** before hydrolysis. The unprecedented *meso* diastereoselectivity of the double anionic thia-*Fries* rearrangement of **5** is a result of coordinating interactions of the lithium cations with oxygen atoms of the product and the diisopropyl-amine nitrogen atom.

Experimental Section

General

The reaction was carried out under inert gas atmosphere (Argon) using *Schlenk* technique and apparatus. THF and hexane were dried at reflux over sodium/benzophenone, dichloromethane by stirring over calcium hydride, and diisopropylamine (DIPA) by stirring over potassium hydroxide. All solvents were freshly distilled before use. For crystallization, the solvents were further degassed using pumping-freeze-thaw technique. CD_2Cl_2 was first dried over molecular sieves (4 Å) for 24 h followed by reflux over CaH_2 and distillation under argon atmosphere collected in a *Schlenk* flask with molecular sieves (4 Å). IR: *Fourier* transform infrared spectrophotometer *Shimadzu IRAffinity-1S* with quest ATR unit (32 scans). Signal intensities: strong (*s*), medium (*m*), weak (*w*), broad (br.). ^{1}H-NMR: *Bruker Ascend* (600.1 MHz) with *Avance NEO Console* at 298 K. The chemical shift of the residual solvent signal of the deuterated solvent (CD_2Cl_2: $\delta = 5.32$ ppm) was used as the internal standard. ^{13}C-NMR: *Bruker Ascend* (151 MHz) with *Avance NEO Console* at 298 K. The chemical shift of the residual solvent signal of the deuterated solvent (CD_2Cl_2: $\delta = 54.00$ ppm) was used as the internal standard. ^{19}F-NMR: *Bruker Ascend* (376.5 MHz) with *Avance III Console* at 298 K. Fluorobenzene was used as the standard (C_6H_5F: $\delta = -113.11$ ppm).

Lithium 2-(trifluoromethylsulfonyl)ferrocenolate (**3**). At $-78\,°C$, LDA in THF (prepared from 2.5 M butyllithium (0.54 mL, 1.34 mmol) in hexane and diisopropylamine (0.57 mL, 4.0 mmol) in THF (3 mL)) was added dropwise to a solution of ferrocenyl triflate

(**1**) in THF (4 mL). The color changed from light yellow to red. The solution was stirred for 20 min at $-78\,°C$. The solvent was removed at reduced pressure, and the remaining red solid was washed with hexane (3×5 mL). The solid was dissolved in dichloromethane and filtered through a *P4* frit into a *Schlenk* flask. The solvent was removed at reduced pressure affording **3** (437 mg, 1.29 mmol, 96%) as a red solid. ^{1}H-NMR (600 MHz, CD_2Cl_2): 4.49 (*s*, 5 H, $C_{Cp}H$); 4.43–4.45 (*m*, 1 H, $C_{Cp}H$); 4.43 (*t*, 1 H, $C_{Cp}H$, $J = 2.9$), 4.38–4.40 (*m*, 1 H, $C_{Cp}H$). ^{13}C-NMR (151 MHz, CD_2Cl_2): 60.68 ($C_{Cp}S$); 61.59 ($C_{Cp}H$); 62.95 ($C_{Cp}H$); 67.16 ($C_{Cp}H$); 71.63 (5 $C_{Cp}H$); 119.6 (*q*, CF_3, $J = 325$); 135.7 ($C_{Cp}O$). ^{19}F-NMR (376 MHz, CD_2Cl_2): -80.5 (*s*, CF_3). IR: 3611*w*, 1647*w*, 1463*s*, 1379*m*, 1329*m*, 1203*s*, 1175*s*, 1123*m*, 1080 *m*, 1003 *m*, 849*w*, 738*w*, 712*m*, 604*s*, 563*m*, 507*m*.

Crystal Structure Analysis: CCDC-2046411. Single crystals suitable for X-ray crystallographic analysis were obtained from slow diffusion of hexane (5 mL) into dichloromethane solution of **3** (1 mL). $C_{44}H_{32}F_{12}Fe_4Li_4O_{12}S_4$, red block, $M_r = 1360.09$, crystal system orthorhombic, space group P2$_1$2$_1$2$_1$, $a = 14.9657(1)$ Å, $b = 15.2558(1)$ Å, $c = 22.9370(2)$ Å, $\alpha = 90°$, $\beta = 90°$, $\gamma = 90°$, $V = 5236.83(7)$ Å^3, $Z = 4$, $d_{calc} = 1.725$ g cm^{-3}, $\mu = 11.114$ mm^{-1}, crystal size $0.14 \times 0.13 \times 0.09$ mm^3, $F(000) = 2720$, *Bruker KAPPA APEX II CCD* diffractometer, graphite crystal monochromator, $T = 233$ K, Cu-K$_\alpha$ radiation ($\lambda = 1.54187$ Å), $3.48° \leq \theta \leq 65.44°$, index ranges $-17 \leq h \leq 15$, $-17 \leq k \leq 18$, $-26 \leq l \leq 21$, reflections collected/unique 8785/5743, numerical absorption correction, structure solution and refinement with SHELX-97,[15] parameter/restraints 721/0, $R_1 = 0.0470$ [$I > 2\sigma(I)$], $wR_2 = 0.898$ (all data), $S = 0.962$, finals maximum/minimum difference electron density $0.449/-0.513$ eÅ^{-3}.

Theoretical Method Section

CPMD Calculations

Car-Parrinello molecular dynamics were benchmarked using the functionals *Becke-Lee-Yang-Parr* (BLYP)[16,17] and *Perdew-Burke-Ernzerhof* (PBE)[18] with and without *Grimme*'s dispersion correction D2.[19] For BLYP, *Goedecker* pseudopotentials[20] were used for all the atoms, and for PBE, *Troullier–Martins* pseudopotentials[21] were chosen for all the atoms except lithium, for which the *Goedecker* functional was utilized. The best matching functional, PBE, without *Grimme*'s dispersion correction, was used to perform further calculations.

Benchmark

The wavefunction was optimized to the *Born–Oppenheimer* surface and the geometry was relaxed using TEMPCONTROL option: the ionic velocities were set back to zero, whenever the temperature exceeded 100 K. The time step chosen was 4 a.u. (~0.1 fs). The plane-wave cutoff determining the basis set size was set to 70 Rydberg. The simulation cell size was set to same size of the crystal unit cell: $14.9657 \times 15.2558 \times 22.9370$ Å^3 and α, β and γ were set to 90°.

Simulations

Perdew–Burke–Ernzerhof (PBE),[18] was used to perform molecular dynamics calculations starting from the transition state geometry **I** found in *Gaussian*. Troullier-*Martins*[21] pseudopotentials were used for the nitrogen atoms.

MLWF of Intermediate **C**. The PBE[18] functional and the pseudopotentials cited previously were used to perform molecular dynamics calculations starting from *Gaussian* optimized structure **C**. The system was optimized to the *Born-Oppenheimer* surface and a molecular dynamics run was performed for 200 steps. Maximally localized *Wannier* functions were calculated (keywords: DIPOLE DYNAMICS[22–24] WANNIER SAMPLE[25–27]). The simulation cell size was set to $22 \times 22 \times 22$ Å^3 and α, β and γ were set to 90°.

Gaussian calculations.[28] For the *Gaussian* calculations, the following GGA and hybrid functionals were benchmarked (*Grimme*'s dispersion with *Becke-Johnson* damping GD3BJ[29] added was marked with D3 abbreviation); BLYP,[16,17] BLYP-D3,[16,17,29] B3LYP,[16,17,30] B3LYP-D3,[16,17,29,30] PBE0,[18,31,32] PBE0-D3,[18,29,31] wB97XD,[33] PBE[18] and M06.[34] We used LANL2DZ[35–38] and LANL,[35–38] for valence and core electrons of iron, respectively. $6\text{-}311+\text{G}(d,p)$[39–41] was used for all other atoms.

Acknowledgements

Author Contribution Statement

G. M. R. B. performed the experiments, analyzed most of the data and performed the calculations. *I. F.* designed and interpreted the quantum chemical calculations. *H. B.* provided necessary compounds and infrastructure and was the scientific mentor of the project. All three authors equally participated in writing the manuscript.

References

[1] J. P. H. Charmant, A. M. Dyke, G. C. Lloyd-Jones, 'The anionic thia-Fries rearrangement of aryl triflates', *Chem. Commun.* **2003**, 380–381.

[2] Z. Zhao, J. Messinger, U. Schön, R. Wartchow, H. Butenschön, 'Unanticipated formation of *ortho*-sulfone substituted phenols by anionic thia-Fries rearrangement of (aryl triflate)tricarbonylchromium complexes', *Chem. Commun.* **2006**, 3007–3009.

[3] G. Werner, C. W. Lehmann, H. Butenschön, 'The First Anionic Thia-Fries Rearrangements at Ferrocene: Ready Access to Trifluoromethylsulfonyl-Substituted Hydroxyferrocenes and an Extremely High Interannular Stereoinduction between Cyclopentadienyl Ligands', *Adv. Synth. Catal.* **2010**, *352*, 1345–1355.

[4] A. M. Dyke, D. M. Gill, J. N. Harvey, A. J. Hester, G. C. Lloyd-Jones, M. P. Muñoz, I. R. Shepperson, 'Decoupling Deprotonation from Metalation: Thia-Fries Rearrangement', *Angew. Chem. Int. Ed.* **2008**, *47*, 5067–5070.

[5] Y. Ma, R. F. Algera, D. B. Collum, 'Sodium Diisopropylamide in *N,N*-Dimethylethylamine: Reactivity, Selectivity, and Synthetic Utility', *J. Org. Chem.* **2016**, *81*, 11312–11315.

[6] E. M. Arnett, M. A. Nichols, A. T. McPhail, 'Structural and energetic evidence for oxygen-lithium-nitrogen chelation in a model for asymmetric induction', *J. Am. Chem. Soc.* **1990**, *112*, 7059–7060.

[7] E. Weiss, 'Structures of Organo Alkali Metal Complexes and Related Compounds', *Angew. Chem. Int. Ed.* **1993**, *32*, 1501–1523.

[8] J. Niemeyer, G. Kehr, R. Fröhlich, G. Erker, 'Bis("ferrocene-saliminato") group 4 metal complexes: synthesis, structural features and use in homogenous Ziegler–Natta polymerization catalysis', *Dalton Trans.* **2009**, 3731–3741.

[9] C. Nottingham, R. Benson, H. Müller-Bunz, P. J. Guiry, 'Synthesis of Ferrocene Oxazoline N,O ligands and Their Application in Asymmetric Ethyl- and Phenylzinc Additions to Aldehydes', *J. Org. Chem.* **2015**, *80*, 10163–10176.

[10] R. Car, M. Parrinello, 'Unified Approach for Molecular Dynamics and Density-Functional Theory', *Phys. Rev. Lett.* **1985**, *55*, 2471–2474.

[11] 'CPMD', Copyright IBM Corp. 1990–2019, Copyright MPI für Festkörperforschung Stuttgart 1997–2001, http://www.cpmd.org/.

[12] G. Werner, H. Butenschön, 'Anionic Thia-Fries Rearrangements of Electron-Rich Ferrocenes and the Unanticipated Formation of Diferrocenyl Sulfate from 2-(Trimethylsilyl)ferrocenyl Imidazolylsulfonate', *Organometallics* **2013**, *32*, 5798–5809.

[13] E. Weiss, G. Hencken, 'Alkylmetal compounds. XII. Refinement of the crystal structure of methyllithium', *J. Organomet. Chem.* **1970**, *21*, 265–268.

[14] J. C. Slater, 'Atomic Radii in Crystals', *J. Chem. Phys.* **1964**, *41*, 3199–3204.

[15] G. M. Sheldrick, 'SHELX97, Programs for Crystal Structure Analysis', University of Göttingen, Germany, 1997.

[16] A. D. Becke, 'Density-functional exchange-energy approximation with correct asymptotic behavior', *Phys. Rev. A* **1988**, *38*, 3098–3100.

[17] C. Lee, W. Yang, R. G. Parr, 'Development of the Colle-Salvetti correlation-energy formula into a functional of the electron density', *Phys. Rev. B* **1988**, *37*, 785–789.

[18] J. P. Perdew, K. Burke, M. Ernzerhof, 'Generalized Gradient Approximation Made Simple', *Phys. Rev. Lett.* **1996**, *77*, 3865–3868.

[19] S. Grimme, 'Semiempirical GGA-type density functional constructed with a long-range dispersion correction', *J. Comput. Chem.* **2006**, *27*, 1787–1799.

[20] S. Goedecker, M. Teter, J. Hutter, 'Separable dual-space Gaussian pseudopotentials', *Phys. Rev. B* **1996**, *54*, 1703–1710.

[21] N. Troullier, J. L. Martins, 'Efficient pseudopotentials for plane-wave calculations', *Phys. Rev. B* **1991**, *43*, 1993–2006.

[22] R. Resta, 'Theory of electric polarization in crystals', *Ferroelectrics* **1992**, *136*, 51–55.

[23] R. D. King-Smith, D. Vanderbilt, 'Theory of polarization of crystalline solids', *Phys. Rev. B* **1993**, *47*, 1651–1654.

[24] R. Resta, 'Macroscopic polarization in crystalline dielectrics: the geometric phase approach', *Rev. Mod. Phys.* **1994**, *66*, 899–915.

[25] N. Marzari, D. Vanderbilt, 'Maximally localized generalized Wannier functions for composite energy bands', *Phys. Rev. B* **1997**, *56*, 12847–12865.

[26] P. L. Silvestrelli, 'Maximally localized Wannier functions for simulations with supercells of general symmetry', *Phys. Rev. B* **1999**, *59*, 9703–9706.

[27] G. Berghold, C. J. Mundy, A. H. Romero, J. Hutter, M. Parrinello, 'General and efficient algorithms for obtaining maximally localized Wannier functions', *Phys. Rev. B* **2000**, *61*, 10040–10048.

[28] G. W. T. M. J. Frisch, H. B. Schlegel, G. E. Scuseria, M. A. Robb, J. R. Cheeseman, G. Scalmani, V. Barone, G. A. Petersson, H. Nakatsuji, X. Li, M. Caricato, A. V. Marenich, J. Bloino, B. G. Janesko, R. Gomperts, B. Mennucci, H. P. Hratchian, J. V. Ortiz, A. F. Izmaylov, J. L. Sonnenberg, D. Williams-Young, F. Ding, F. Lipparini, F. Egidi, J. Goings, B. Peng, A. Petrone, T. Henderson, D. Ranasinghe, V. G. Zakrzewski, J. Gao, N. Rega, G. Zheng, W. Liang, M. Hada, M. Ehara, K. Toyota, R. Fukuda, J. Hasegawa, M. Ishida, T. Nakajima, Y. Honda, O. Kitao, H. Nakai, T. Vreven, K. Throssell, J. A. Montgomery Jr., J. E. Peralta, F. Ogliaro, M. J. Bearpark, J. J. Heyd, E. N. Brothers, K. N. Kudin, V. N. Staroverov, T. A. Keith, R. Kobayashi, J. Normand, K. Raghavachari, A. P. Rendell, J. C. Burant, S. S. Iyengar, J. Tomasi, M. Cossi, J. M. Millam, M. Klene, C. Adamo, R. Cammi, J. W. Ochterski, R. L. Martin, K. Morokuma, O. Farkas, J. B. Foresman, D. J. Fox,'Gaussian 16, Revision A 03', Gaussian, Inc., Wallingford, CT, 2016.

[29] S. Grimme, J. Antony, S. Ehrlich, H. Krieg, 'A consistent and accurate *ab initio* parametrization of density functional dispersion correction (DFT–D) for the 94 elements H–Pu', *J. Chem. Phys.* **2010**, *132*, 154104.

[30] A. D. Becke, 'A new mixing of Hartree–Fock and local-density functional theories', *J. Chem. Phys.* **1993**, *98*, 1372–1377.

[31] C. Adamo, V. Barone, 'Toward reliable density functional methods without adjustable parameters: the PBE0 model', *J. Chem. Phys.* **1999**, *110*, 6158–6170.

[32] J. P. Perdew, M. Ernzerhof, K. Burke, 'Rationale for mixing exact exchange with density functional approximations', *J. Chem. Phys.* **1996**, *105*, 9982–9985.

[33] J.-D. Chai, M. Head-Gordon, 'Long-range corrected hybrid density functionals with damped atom-atom dispersion corrections', *Phys. Chem. Chem. Phys.* **2008**, *10*, 6615–6620.

[34] Y. Zhao, D. G. Truhlar, 'The M06 suite of density functionals for main group thermochemistry, thermochemical kinetics, noncovalent interactions, excited states, and transition elements: two new functionals and systematic testing of four M06-class functionals and 12 other functionals', *Theor. Chem. Acc.* **2008**, *120*, 215–241.

[35] P. J. Hay, W. R. Wadt, '*Ab initio* effective core potentials for molecular calculations. Potentials for the transition metal atoms Sc to Hg', *J. Chem. Phys.* **1985**, *82*, 270–283.

[36] W. R. Wadt, P. J. Hay, '*Ab initio* effective core potentials for molecular calculations. Potentials for main group elements Na to Bi', *J. Chem. Phys.* **1985**, *82*, 284–298.

[37] P. J. Hay, W. R. Wadt, '*Ab initio* effective core potentials for molecular calculations. Potentials for K to Au including the outermost core orbitals', *J. Chem. Phys.* **1985**, *82*, 299–310.

[38] T. H. Dunning, P. J. Hay, 'Gaussian Basis Sets for Molecular Calculations', in 'Methods of Electronic Structure Theory', Ed. H. F. Schäfer, Springer, Boston, MA, 1977, Vol. 3, pp. 1–27.

[39] A. D. McLean, G. S. Chandler, 'Contracted Gaussian basis sets for molecular calculations. I. Second row atoms, $Z = 11–18$', *J. Chem. Phys.* **1980**, *72*, 5639–5648.

[40] R. Krishnan, J. S. Binkley, R. Seeger, J. A. Pople, 'Self-consistent molecular orbital methods. XX. A basis set for correlated wave functions', *J. Chem. Phys.* **1980**, *72*, 650–654.

[41] M. J. Frisch, J. A. Pople, J. S. Binkley, 'Self-consistent molecular orbital methods. 25. Supplementary functions for Gaussian basis sets', *J. Chem. Phys.* **1984**, *80*, 3265–3269.